Article

Journal of
Nanoscience and Nanotechnology
Vol. 18, 4884–4890, 2018
www.aspbs.com/jnn

Fabrication of Porous ZnO/Co_3O_4 Composites for Improving Cycling Stability of Supercapacitors

Dongqing Su[1], Longmei Zhang[1], Zehua Tang[1], Tingting Yu[1], Huili Liu[1], Junhao Zhang[1,2,*], Yuanjun Liu[1], Aihua Yuan[1,2,*], and Qinghong Kong[3]

[1] School of Environmental and Chemical Engineering, Jiangsu University of Science and Technology, Zhenjiang, Jiangsu 212003, China
[2] Marine Equipment and Technology Institute, Jiangsu University of Science and Technology, Zhenjiang, Jiangsu 212003, China
[3] School of the Environment and Safety Engineering, Jiangsu University, Zhenjiang, Jiangsu 212013, China

To tackle the issue of poor cycling stability for metal oxide nanoparticles as supercapacitor electrode, porous ZnO/Co_3O_4 composites were fabricated via solid-state thermolysis of [CoZn(BTC)(NO_3)]($2H_2O$)(0.5DMF) under air atmosphere. The results demonstrate that the products are mesoporous polyhedron structure with the diameter of about 10 μm, which are constructed by many interconnected nanocrystals with the sizes of around 20 nm. ZnO/Co_3O_4 composites as supercapacitor electrode exhibited excellent cyclic stability capacity, showing a maximum specific capacitance of 106.7 F g^{-1} and a capacity retention of 102.7 F·g^{-1} after 1000 cycles at 0.5 A·g^{-1}. The superior electrochemical performance was contributed to ZnO/Co_3O_4 composites with porous structures and small size, which shortened the route of electronic transmission as well as ions insertion and desertion processes. Additionally, the synergetic effect of bimetallic oxides improved the electrochemical stability.

Keywords: Metal Organic Framework, ZnO/Co_3O_4 Composites, Porous Structure, Supercapacitors, Cycling Stability.

1. INTRODUCTION

Electrochemical energy storage has drawn considerable attention in enabling utilization of renewable electricity generation due to climate change and decreasing availability of fossil fuels.[1,2] As an electrochemical energy storage device, supercapacitors (SCs) have many outstanding features, for instance high power density, long life span and fast recharge features.[3] Moreover, the performance of SCs has been greatly improved, as electrode materials have been tuned at the nanoscale and electrolytes have gained an active role currently in storing more energy than conventional capacitors and providing higher power than batteries.[4] With more rigorous requirements for hybrid electric vehicles, laptops, smart phones, and cameras, the energy density of SCs should be substantially increased without deteriorating the power density or cycle life.[5–7]

Among the electrode materials for supercapacitor applications, extensive attention has been paid to investigate pseudocapacitive transition metal oxides, such as MnO_2,[8] Fe_3O_4,[9] CuO,[10] NiO,[11] SnO_2,[12] and Co_3O_4.[13] Among this wide variety of materials, Co_3O_4 has attracted significant attention and become one of the most important functional materials due to its environmental friendliness, low cost, and favorable pseudocapacitive characteristics. However, the applications of Co_3O_4 can be barely effectively utilized to SCs due to large volume expansion during electrochemical reactions, which results in poor intrinsic electrical cyclability.[14] Therefore, it is far from meeting the ever-growing requirements of the next-generation supercapacitors.

Recently, bimetallic oxides have attracted extensive interest for their enhanced characteristics over the single metallic oxide.[15] Zinc and/or Co oxides, being cost-effective, abundant resources, environmental benign nature, and as well as excellent thermal stabilities, are a kind of promising materials that have wide applications in supercapacitors,[16] lithium-ion batteries,[17] and gas sensors.[18] To enhance the electrochemical properties, exploring mild strategies to synthesize bimetallic oxides with porous structures is very important. Recently, Metal-organic frameworks (MOFs) have been demonstrated as ideal metal, carbon and other

*Authors to whom correspondence should be addressed.

 1533-4880/2018/18/4884/007 doi:10.1166/jnn.2018.15289

element sources, and self-sacrificial templates for the preparation of porous metal oxide or carbon matrix composites.[19, 20] Compared with other templates, MOFs provide some superiority related to their robust morphology and large porosity. In addition, the morphology of MOFs could be preserved in the obtained materials. In this work, porous ZnO/Co_3O_4 composites were prepared by a simple calcination of Zn, Co-MOF ($[CoZn(BTC)(NO_3)](2H_2O)(0.5DMF)$) precursor in air atmosphere. The presence of Co^{3+} ions mitigates the Jahn-Teller effect of Zn^{2+} ions and thus stabilizes the bimetallic framework for long-term cycling, which exhibits rapid electron transfer pathways with better redox reactions.[21] On the other hands, the presence of Zn^{2+} suppresses the redox activity of Co for improving the stability of the electrode. The porous ZnO/Co_3O_4 composites are promising electrode materials for electrochemical supercapacitors, showing a specific capacitance of 167 F g^{-1} at a current density of 0.5 A g^{-1}. More importantly, the cycle stability was remarkable improved due to the synergetic effect of two kinds of metal oxides. A reversible capacity of 102.7 F g^{-1} was maintained, and the capacity retentions are nearly 100% at 0.5 A g^{-1} after 1000 cycles. These encouraging results show great potential in terms of developing high-capacitive energy storage devices for practical applications.

2. EXPERIMENTAL SECTION

2.1. Chemicals

Zinc nitrate hexahydrate ($Zn(NO_3)_2 \cdot 6H_2O$, ≥99.0%), Pyrazine ($C_4H_4N_2$, ≥99.0%), cobalt nitrate hexahydrate ($Co(NO_3)_2 \cdot 6H_2O$, ≥98.0%), polyvinylpyrrolidone (PVP, average MW: 10000), 1,3,5-benzenetricarboxylic acid, and *N*,*N*-dimethylformamide were purchased from commercial suppliers (J&K reagent Co., Ltd.). All the chemicals were used without further purification.

2.2. Preparation of Zn, Co-MOF Crystal

In a typical solvothermal procedure, 0.3 mmol 1,3,5-benzenetricarboxylic acid with 1.5 mmol · L^{-1} pyrazine, 0.3 mmol $Co(NO_3)_2 \cdot 6H_2O$ and 0.3 mmol $Zn(NO_3)_2 \cdot 6H_2O$ were dissolved in 15 mL *N*,*N*-dimethylformamide (DMF) with stirring at room temperature. After stirring for 10 min, the homogeneous solution was transformed into a Teflon-lined stainless steel autoclave with 50 mL capacity, and was kept at 100 °C for 24 h. After cooling to room temperature, the precipitation was washed with ethanol and alcohol for several times, and then dried in a vacuum at 50 °C for 12 h and obtained pink crystal precursor. The above-synthesized precursor was put into a ceramic crucible and then heated to different temperature with a heating rate 1 °C · min^{-1}, and maintained at the corresponding temperature for 30 minutes under air atmosphere to obtain porous ZnO/Co_3O_4 composites. The samples at different calcination temperatures (400, 500, 600 °C) were prepared for electrochemical performance test.

2.3. Characterization

The Fourier transform infrared (FTIR) spectrum of Zn, Co-MOF precursor was recorded on a Bruker Vector 22 spectrometer ranging from 4000–400 cm^{-1}. Powder X-ray diffraction (XRD) patterns were obtained on a Shimadzu XRD-6000 diffractometer using Cu-Kαg radiation (0.15406 nm). The field-emission scanning electron microscopy (FESEM) was performed on a ZEISS Merlin Compact and JEOL JEM-2100F. The elemental analysis was carried out with an energy-dispersive X-ray spectrometer (EDS, Oxford X-Max). The nitrogen adsorption–desorption isotherms and textural properties were determined on a Micromeritics Instrument Corporation sorption analyzer (ASAP2020). The thermogravimetric analysis (TGA) was carried out using a Mettler Toledo TGA/SDTA851 thermal analyzer under nitrogen atmosphere with a heating rate of 10 °C · min^{-1}.

2.4. Electrochemical Measurements

All electrochemical measurements were performed on an Autolab PGSTAT302N potentiost at (Eco-Chemie) and tested in a standard three-electrode configuration equipped with a platinum plate and saturated calomel electrode (SCE) as the counter and reference electrodes, respectively. The working electrodes were fabricated according to the following process. The as-prepared material, carbon black and poly(vinylidenefluoride) (PVDF) were mixed with a mass ratio of 8:1:1 and dispersed in *N*-methyl-2-pyrrolidone (NMP). As a comparison, working electrodes of ZnO/Co_3O_4 nanoparticles at different calcination temperature were fabricated by the above mentioned process. The as-made slurry was coated onto the graphite paper of about 1 cm^2 and dried at 60 °C in 12 h. The area specific capacitance of the electrode is calculated from the discharge process according to the following equation:

$$C = \frac{It}{\Delta V m}$$

where C (F g^{-1}) is the specific capacitance, I is the discharge current, t is the total discharge time, ΔV is the potential drop during discharge, and m is the mass of active materials in a single electrode, respectively. In this work, different concentration of alkaline hydroxides aqueous solution was utilized as the electrolyte and all measurements were performed at 298 K. The electrochemical performances of electrodes were characterized by cyclic voltammetry (CV) and galvanostatic charge–discharge (GCD) tests within a potential range from 0 to 0.5 V versus SCE at different scan rates and current densities. The electrochemical impedance spectroscopy (EIS) measurement was carried out in the frequency range from 0.01 Hz to 100 kHz at open circuit potential with an AC perturbation of 10 mV.

3. RESULTS AND DISCUSSION

The FTIR spectrum of Zn, Co-MOF precursor was carried out at room temperature, as shown in Figure 1(a). Four distinct characteristic absorption peaks at 1636, 1573, 1453, 1376 cm^{-1} are attributed to the antisymmetric stretching vibration and symmetric stretching vibrations from the C═C of 1,3,5-benzentricarboxylic acid. The weak peak around 1109 cm^{-1} is ascribed to C–O stretching vibration.[22] The strong and broad peak at 3455 cm^{-1} is assigned to O–H stretching vibration, suggesting that the O–H of the carboxylate groups is partly deprotonated, which indicates that the COO– of H_3BTC coordinates to Zn or Co in a monodentate mode. What's more, Figure 1(b) displays the XRD pattern of as prepared Zn, Co-MOF, which is consistent well with the simulated pattern based on the crystal structure with $[CoZn(BTC)(NO_3)](2H_2O)(0.5DMF)$, and confirms that the formula of the MOF precursor is $[CoZn(BTC)(NO_3)](2H_2O)(0.5DMF)$.[20] The thermal stability of the precursor was performed by TGA under air atmosphere, as shown in Figure 1(c). The results indicate that the weight loss of Zn, Co-MOF precursor includes a slow weight loss (18.14%) from 100–375 °C and a fast weight loss (51.68%) from 375–610 °C. The little weight loss before 150 °C indicates that there are little amount of crystal water in Zn, Co-MOF, and the weight loss from 150 °C to 375 °C is attributed to the release of DMF. From 375–610 °C, the weight loss (51.68%) can be ascribed to the decomposition of complex and subsequent oxidation of ligands, which is similar to the theoretical value of $[CoZn(BTC)(NO_3)](2H_2O)(0.5DMF)$.[20] Figure 1(d) shows the XRD pattern of the product by calcining the precursor at 400 °C for 30 min in air. The diffraction peaks at 2θ values of 18.8, 31.0, 36.5, 38.2, 44.4, 55.1, 58.8, 64.6, and 73.4°, corresponding to (111), (220), (311), (222), (400), (422), (511), (440) and (620), respectively, can be readily indexed to hexagonal ZnO (PDF no. 79-2205). The diffraction peaks at 2θ values of 31.8, 34.4, 36.3, 47.5, 56.6, 62.9, 66.4, 67.9, 69.1 and 77.0°, denoted as (100), (002), (101), (102), (110), (103), (200), (112), (201) and (202), are indexed to Co_3O_4 (JCPDS no.75-1621). No other impurity peaks were detected, revealing that Zn, Co-MOF precursor was converted completely to ZnO/Co_3O_4 composites. Additionally, the broaden diffraction peaks indicate that the ZnO/Co_3O_4 composites are composed of numerous nanoparticles with small size. Therefore, it can be concluded that the thermal decomposition of $[CoZn(BTC)(NO_3)](2H_2O)(0.5DMF)$ was complete and Co_3O_4/ZnO was formed by the decomposition of the precursors. This also explains how the porous architectures developed. These decomposition reactions are as follows:

In order to investigate the effect of Zn, Co-MOF as sacrificial templates for the morphologies of the product,

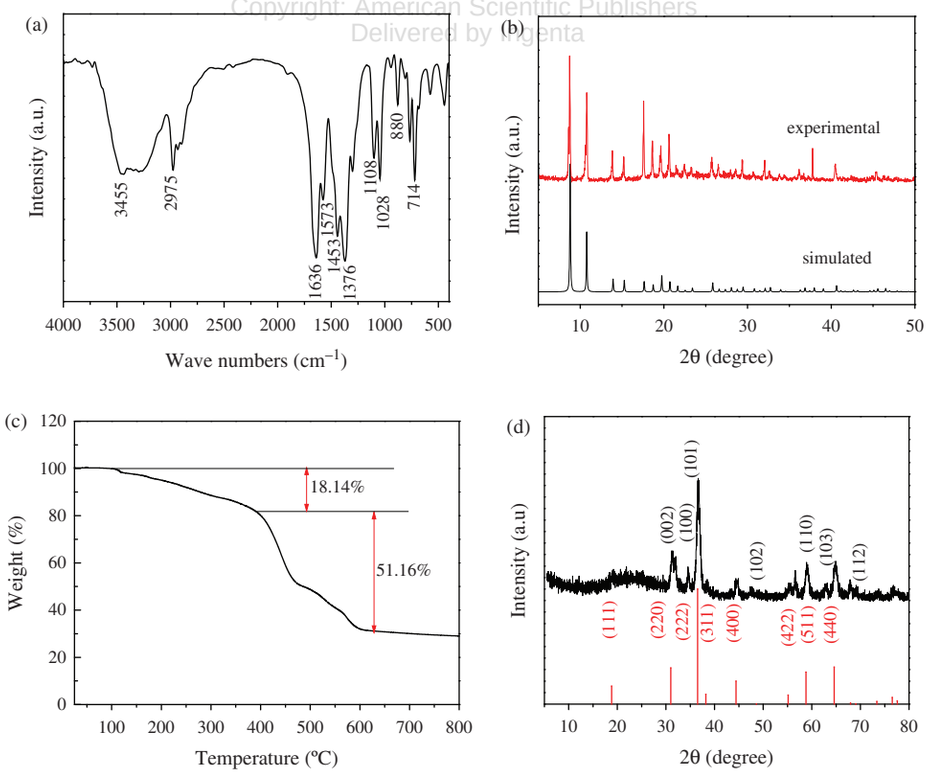

Figure 1. (a) FTIR spectra of Zn, Co-MOF; (b) XRD patterns of Zn, Co-MOF; (c) TGA curve of Zn, Co-MOF in air atmosphere at a heating rate of 10 °C · min^{-1}; (d) XRD pattern of ZnO/Co_3O_4 composites.

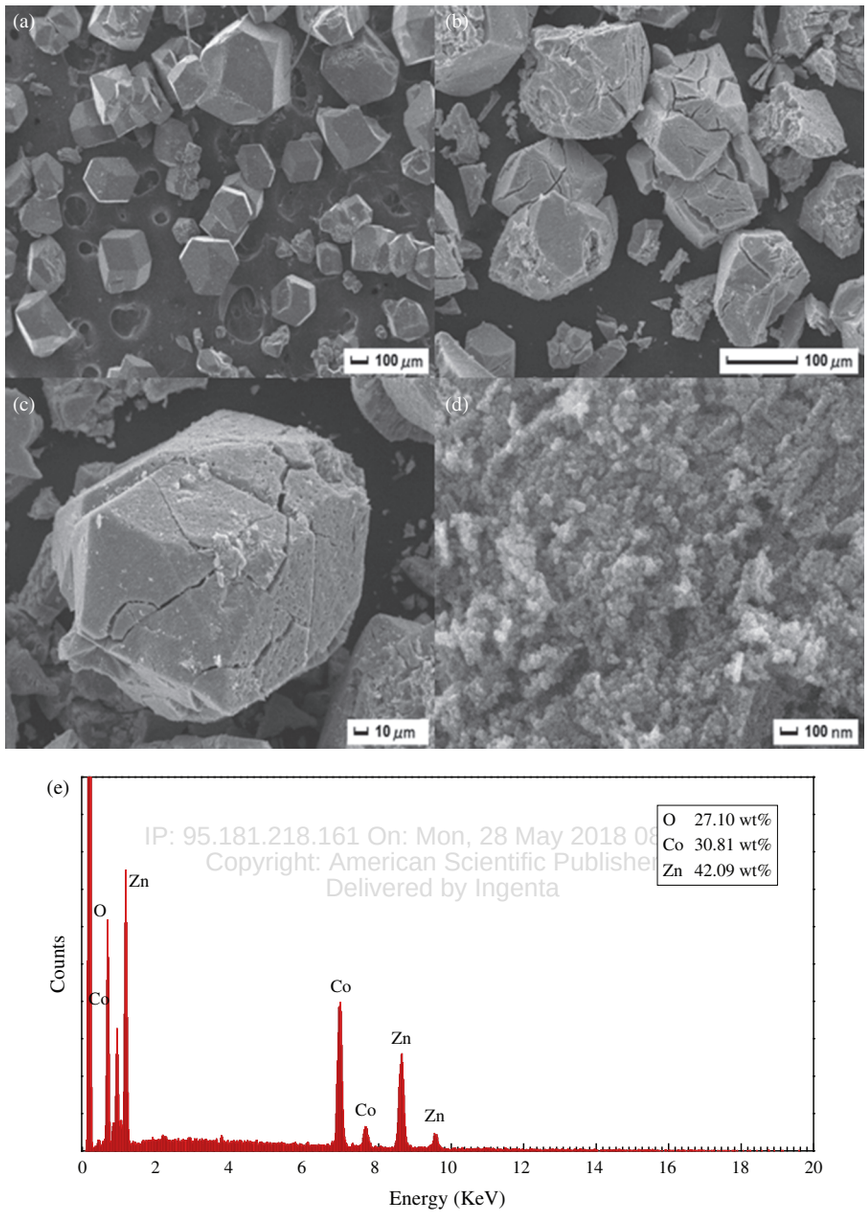

Figure 2. (a) SEM images of Zn, Co-MOF precursor; (b–d) SEM images of ZnO/Co_3O_4 composites; (e) EDX spectrum of ZnO/Co_3O_4 composites.

FESEM images of Zn, Co-MOF and ZnO/Co_3O_4 composites are illustrated in Figure 2. From the results in Figure 2(a), a large amount of relatively uniform polyhedral crystals with an average diameter of about 300 μm was obtained by a simple solvothermal method. It is clear to see porous nature from Figure 2(b), which is resulted from the successive release of CO_2, H_2O and N_xO_y during the thermal decomposition. After the pyrolysis of Zn, Co-MOF with air atmosphere at 400 °C for 3 h, the product substantially retained the original morphology of original Zn, Co-MOF. Nevertheless, the surface became rough and concave, the structure appeared remarkable shrinkage. This could be associated with the massive loss of organic components during the annealing process. Careful observation displays that ZnO/Co_3O_4 composites are assembled by numerous nanoparticles with the size of ~20 nm.

$$[CoZn(BTC)(NO_3)](2H_2O)(0.5DMF)$$
$$\xrightarrow{\Delta} Co_3O_4 + ZnO + H_2O + CO_2 + NO_2$$

It is clear the ZnO/Co_3O_4 composites structural retention is preserved at larger scale from Figure 2(c). Additionally, the EDX spectrum in Figure 2(e) further confirm that the products contain Zn, Co, O elements with their weight percent, and no other elements are detected, which are consistent with the results of XRD.

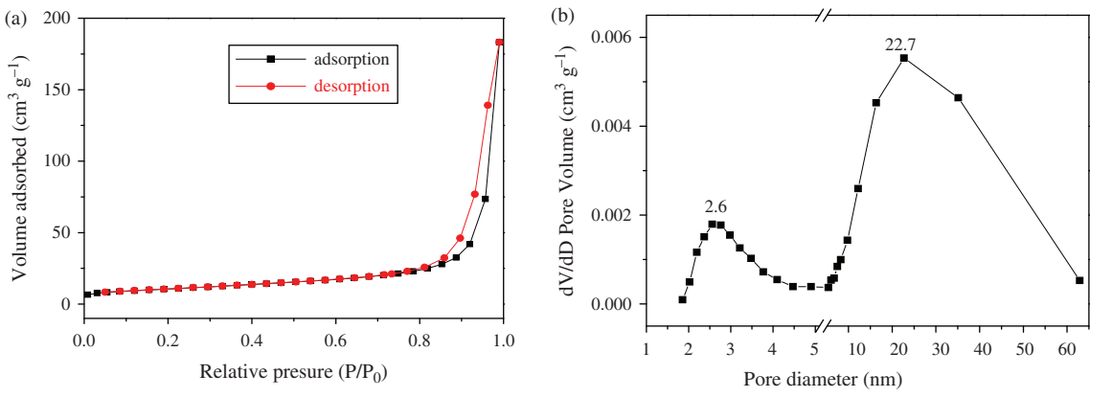

Figure 3. (a) N_2 adsorption and desorption isotherm of ZnO/Co_3O_4 composites; (b) pore size distribution of ZnO/Co_3O_4 composites.

The surface profile is the key factor for the electroactive materials in electrical storage applications, as can be observed from Figure 3(a), the N_2 adsorption quantity of ZnO/Co_3O_4 increased when the relative pressure was raised, which is very common in porous materials. The calculated results of the BET specific surface area is 37.2 $m^2 \cdot g^{-1}$ for the ZnO/Co_3O_4 porous material. The pore sizes can be seen from Figure 3(b), it is clear that the peak at 2.6 nm on the pore size distribution curves are narrow, which shows that the pore sizes are uniform. The pore size of ZnO/Co_3O_4 composites derived from the adsorption branch using the BJH method are centered at about 22.7 nm, however the pore size distribution curves are broad. According to the morphology and structure characteristic, the pore structures can be attributed to the decomposition process that the ligands were removed and resulted in the formation of small pores.[24] The larger surface area can offer more active sites for the electrochemical reactions and ensure an efficient transport pathway between the electrolyte and active electrode materials.

Considering that porous ZnO/Co_3O_4 composites show some advantageous features for supercapacitor application, the electrochemical behaviors were evaluated by CV, GCD and ESI. Figure 4 presents electrochemical performances of ZnO/Co_3O_4 composites in KOH electrolyte with different concentration at the scan rate 10 mV s^{-1}, which clearly demonstrates that the highest specific capacity (106 F g^{-1}) was obtained when 6 mol L^{-1} KOH solution was used. According to the results, calcination temperature also has certain impact for the specific capacity of the supercapacitor, as shown in Figure 5. The specific capacity of the product by calcination at 400 °C is higher than those of the products by calcination at 500 °C and 600 °C, which may be attributed to that the product at 400 °C has better conductivity.

Based on the above discussion, the ZnO/Co_3O_4 composites were selected as by calcination at 400 °C and the electrochemical performances were investigated using three-electrode mode by CV and GCD testing in 6 mol L^{-1} KOH electrolyte. The representative CV curves at different scan rates are shown in Figure 6(a), which present an approximately symmetric shape, indicating the pseudocapacitive nature with fast charge/discharge processes. A distinct pair of well-defined redox peaks is observed within the potential range −0.1–0.5 V (vs. SCE), which clearly indicates that the electrochemical capacity mainly results from pseudocapacitance behavior by two faradic redox reactions. With the scan rate increase from 5 to 20 mV s^{-1},

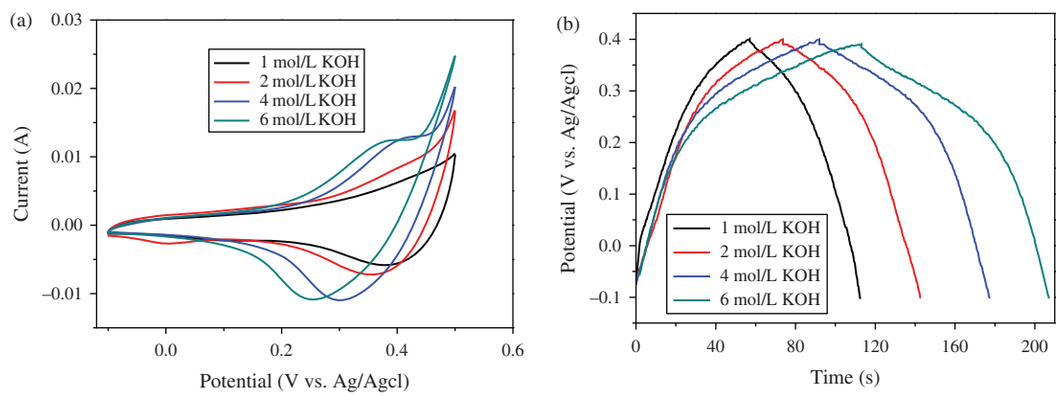

Figure 4. (a) CV curves of the porous ZnO/Co_3O_4 electrode in KOH electrolyte with different concentration at scan rates of 10 mV s^{-1}. (b) GCD curves of the porous ZnO/Co_3O_4 electrode in KOH electrolyte with different concentration at current densities of 0.5 A g^{-1}.

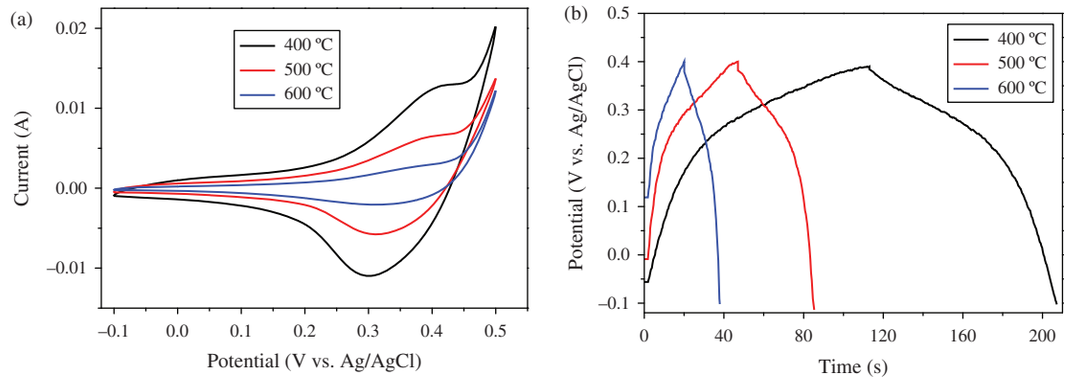

Figure 5. (a) CV curves of the porous ZnO/Co_3O_4 electrode in 6 mol L^{-1} KOH electrolyte at different calcinaton temperatures; (b) GCD curves of the porous ZnO/Co_3O_4 electrode in 6 mol L^{-1} KOH electrolyte at different calcination temperatures.

the increased peak current suggests that there is a good reversibility during the fast charge–discharge process.[25] To further evaluate the potential application of the porous ZnO/Co_3O_4 composites as electrode for ECs, Figure 6(b) presents the GCD curves in 6 mol $\cdot L^{-1}$ KOH electrolyte between 0.0 and 0.4 V at various current densities ranging from 0.5 to 3 A g^{-1}, and the specific capacitances are 106.7 F g^{-1}, 83.3 F g^{-1}, 44.4 F g^{-1}, 21.1 F $\cdot g^{-1}$, which was caused by the resistance increase in ZnO/Co_3O_4 composites and the relatively insufficient faradic redox reaction at higher current densities. The nonlinear charge–discharge profiles further verify the pseudocapacitance behavior. Figure 6(c) displays the cycling performance of the porous ZnO/Co_3O_4 electrode at 0.5 A g^{-1}. After 1000 cycles, the specific capacitance still had a reversible discharge capacity of 102.7 F g^{-1}, and the capacity retention was nearly 100% compared with that of the first discharge capacity. The excellent cycling stability

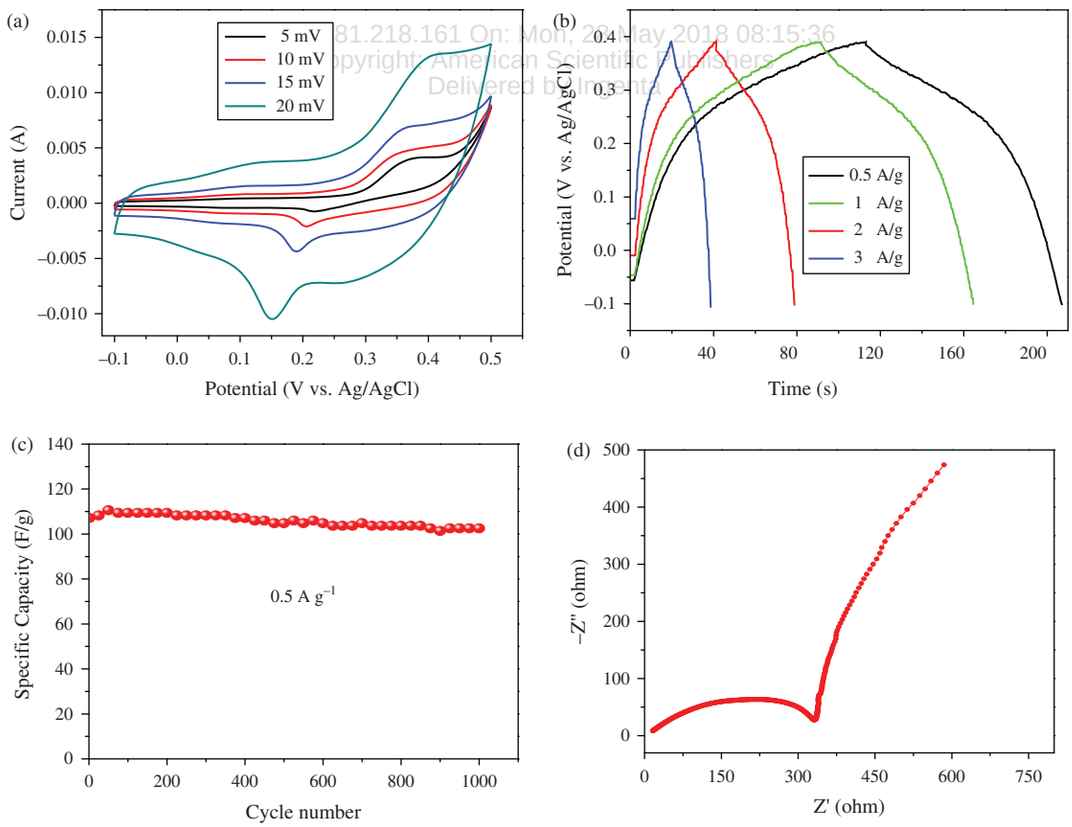

Figure 6. Electrochemical performances of ZnO/Co_3O_4 electrode calcinated at 400 °C in 6 mol L^{-1} KOH electrolyte: (a) CV curves at various scan rates; (b) GCD curves at different current densities; (c) cycling performance at 0.5 A g^{-1}; (d) nyquist plot of ZnO/Co_3O_4 electrode.

is attributed to that the specific porous structure of the porous ZnO/Co_3O_4 electrode can serve as a robust reservoir for ions, and enhance the diffusion kinetics. The porous channels ensure efficient contact between the electrolyte and the surface of the electroactive particles. Moreover, the porous structures lead to higher specific surface area, which can provide many surface electroactive sites for redox pseudocapacitance and further improves the surface adsorption–desorption process of alkali cations. The advantageous high porosity can also shorten the ion transport/diffusion path that leads to fast kinetics for both electrons and ions within the oxides, resulting in reduced internal resistance and improved high-power performance.[26–28] To further understand the above electrochemical performances, Nyquist plot of porous ZnO/Co_3O_4 electrode was investigated at fresh electrode, as shown in Figure 6(d).[29]

4. CONCLUSION

In summary, ZnO/Co_3O_4 composites were prepared on a large scale via solid-state thermolysis from Zn, Co-MOF crystal. The results revealed that the porous ZnO/Co_3O_4 composites are assembled by numerous nanoparticles with the size of ~20 nm, and possess hierarchical porosity with high BET surface area of 37.2 $m^2\ g^{-1}$. Serving as an electrode material for supercapacitors, it exhibits excellent pseudocapacitance performance with a maximum specific capacitance of 106.7 F g^{-1} and a capacity retention of 102.7 $F \cdot g^1$ after 1000 cycles at 0.5 A g^{-1}. The fascinating performances can be attributed to the improvement of pseudocapacitive reaction by porous ZnO/Co_3O_4 electrode. It is expected that the facile solid-phase conversion approach can be viable extended to prepare other porous metal oxide-based functional materials with well-defined morphologies.

Acknowledgment: The work was financially supported by Natural Science of Foundation of China (Nos. 51672114, 51603091), Natural Science Foundation of Jiangsu Province (No. BK 20150505), the Open Project Program of Key Laboratory of Eco-textiles, Ministry of Education, Jiangnan University (No. KLET1609), the China Postdoctoral Science Foundation (No. 2017M611747), Foundation from Marine Equipment and Technology Institute for Jiangsu university of Science and Technology (No. HZ20170015), and Qinglan Project of Jiangsu Province.

References and Notes

1. M. Z. Ge, Q. S. Li, C. Y. Cao, J. Y. Huang, S. H. Li, S. N. Zhang, Z. Chen, K. Q. Zhang, and S. S. Ai-Deyab, *Adv. Sci.* 4, 1600152 (**2017**).
2. J. H. Zhang, M. Huang, B. J. Xi, K. Mi, A. H. Yuan, and S. L. Xiong, *Adv. Energy Mater.* (**2017**), DOI: 10.1002/aenm.201701330.
3. A. H. Khan, S. Ghosh, B. Pradhan, A. Dalui, L. K. Shrestha, S. Acharya, and K. Ariga, *Bull. Chem. Soc. Jpn.* 90, 627 (**2017**).
4. D. Ji, H. Zhou, Y. Y. Dan, H. X. Yang, and A. H. Yuan, *J. Mater. Chem. A* 4, 8283 (**2016**).
5. M. Huang, K. Mi, J. H. Zhang, H. L. Liu, T. T. Yu, A. H. Yuan, Q. H. Kong, and S. L. Xiong, *J. Mater. Chem. A* 5, 266 (**2016**).
6. H. L. Liu, T. T. Yu, D. Q. Su, Z. H. Tang, J. H. Zhang, Y. J. Liu, A. H. Yuan, and Q. H. Kong, *Ceram. Int.* 43, 14395 (**2017**).
7. M. S. Kim, E. Lim, S. Kim, C. Jo, J. Chun, and J. Lee, *Adv. Funct. Mater.* 27, 1603921 (**2016**).
8. M. Kim, Y. Hwang, and J. Kim, *J. Mater. Sci.* 48, 7652 (**2013**).
9. V. D. Nithya and N. S. Arul, *J. Mater. Chem. A* 4, 10767 (**2016**).
10. J. Zhang, H. J. Feng, Q. Qin, G. F. Zhang, Y. X. Cui, Z. Z. Chai, and W. J. Zheng, *J. Mater. Chem. A* 4, 6357 (**2016**).
11. L. Liu, H. Guo, J. Liu, F. Qian, T. Li, W. Chen, X. Yang, and Y. Guo, *Chem. Commun.* 50, 9485 (**2014**).
12. Z. A. Hu, Y. L. Xie, Y. X. Wang, L. P. Mo, Y. Y. Yang, and Z. Y. Zhang, *Mater. Chem. Phys.* 114, 990 (**2009**).
13. K. Deori, S. K. Ujjain, R. K. Sharma, and S. Deka, *ACS Appl. Mater. Interfaces* 5, 10665 (**2013**).
14. S. Abouali, M. A. Garakani, B. Zhang, Z. L. Xu, E. K. Heidari, J. Q. Huang, and J. K. Kim, *ACS Appl. Mater. Interfaces* 7, 13503 (**2015**).
15. L. M. Zhang, J. H. Zhang, Y. J. Liu, L. Zhang, and A. H. Yuan, *J. Nanosci. Nanotechnol.* 17, 2571 (**2017**).
16. M. Salanne, B. Rotenberg, K. Naoi, K. Kaneko, P. L. Taberna, C. P. Grey, B. Dunn, and P. Simon, *Nat. Energy* 1, 16070 (**2016**).
17. P. Poizot, S. Laruelle, S. Grugeon, L. Dupont, and J. M. Tarascon, *Nature* 32, 496 (**2000**).
18. M. Drobek, J. H. Kim, M. Bechelany, C. Vallicari, A. Julbe, and S. S. Kim, *ACS Appl. Mater. Interfaces* 8, 8323 (**2016**).
19. D. Tian, X. L. Zhou, Y. H. Zhang, Z. Zhou, and X. H. Bu, *Inorg. Chem.* 54, 8159 (**2015**).
20. L. M. Zhang, B. Yan, J. H. Zhang, Y. J. Liu, A. H. Yuan, and G. Yang, *Ceram. Int.* 42, 5160 (**2016**).
21. R. J. Elliott, *J. Lumin.* s31–32, 29 (**2015**).
22. J. H. Zhang, Q. H. Kong, L. W. Yang, and D. Y. Wang, *Green Chem.* 18, 3066 (**2016**).
23. J. S. Chen, T. Zhu, Q. H. Hu, J. J. Gao, F. B. Su, S. Z. Qiao, and X. W. Lou, *ACS Appl. Mater. Interfaces* 2, 3628 (**2010**).
24. E. Yamamoto and K. Kuroda, *Bull. Chem. Soc. Jpn.* 89, 501 (**2016**).
25. L. B. Kong, J. W. Lang, M. Liu, Y. C. Luo, and L. Kang, *J. Power Sources* 194, 1194 (**2009**).
26. C. Y. Liu, S. L. Zhao, Y. N. Lu, Y. X. Chang, D. D. Xu, Q. Wang, Z. H. Dai, J. C. Bao, and M. Han, *Small* 13, 1603494 (**2017**).
27. D. Ji, H. Zhou, Y. L. Tong, J. P. Wang, M. Z. Zhu, T. H. Chen, and A. H. Yuan, *Chem. Eng. J.* 313, 1623 (**2017**).
28. K. S. Lakhi, D. H. Park, K. Al-Bahily, W. Cha, B. Viswanathanm, J. H. Choy, and A. Vinu, *Chem. Soc. Rev.* 46, 72 (**2017**).
29. J. H. Zhang, S. Wan, B. Yan, L. B. Wang, and Y. T. Qian, *J. Nanosci. Nanotechnol.* 13, 4364 (**2013**).

Received: 4 July 2017. Accepted: 9 August 2017.